

TRACING THE MAGNETIC FIELD MORPHOLOGY OF THE LUPUS I MOLECULAR CLOUD*

G. A. P. FRANCO

Departamento de Física – ICEx – UFMG, Caixa Postal 702, 30.123-970 Belo Horizonte, Brazil; franco@fisica.ufmg.br

AND

F. O. ALVES

Max-Planck-Institut für extraterrestrische Physik, Giessenbachstr. 1, D-85748 Garching, Germany; falves@mpe.mpg.de

Draft version November 27, 2017

ABSTRACT

Deep *R*-band CCD linear polarimetry collected for fields with lines-of-sight toward the Lupus I molecular cloud is used to investigate the properties of the magnetic field within this molecular cloud. The observed sample contains about 7000 stars, almost 2000 of them with polarization signal-to-noise ratio larger than 5. These data cover almost the entire main molecular cloud and also sample two diffuse infrared patches in the neighborhood of Lupus I. The large scale pattern of the plane-of-sky projection of the magnetic field is perpendicular to the main axis of Lupus I, but parallel to the two diffuse infrared patches. A detailed analysis of our polarization data combined with the *Herschel*/SPIRE 350 μm dust emission map shows that the principal filament of Lupus I is constituted by three main clumps acted by magnetic fields having different large-scale structure properties. These differences may be the reason for the observed distribution of pre- and protostellar objects along the molecular cloud and its apparent evolutive stage. On the other hand, assuming that the magnetic field is composed by a large-scale and a turbulent components, we find that the latter is rather similar in all three clumps. The estimated plane-of-sky component of the large-scale magnetic field ranges from about 70 μG to 200 μG in these clumps. The intensity increases towards the Galactic plane. The mass-to-magnetic flux ratio is much smaller than unity, implying that Lupus I is magnetically supported on large scales.

Subject headings: ISM: clouds – ISM: individual objects: Lupus I – ISM: magnetic fields – Techniques: polarimetry

1. INTRODUCTION

The shape of an interstellar cloud may provide a wealth of information on the mechanisms that govern cloud formation and evolution. In the past decades, there were accumulated evidences that the interstellar medium (ISM) has a filamentary appearance. The *IRAS* all sky survey revealed a profusion of parsec-scale filaments in the diffuse ISM (Low et al. 1984), while observations of dust emission, interstellar reddening, and molecular gas emission have shown that filaments are also omnipresent in the Galactic molecular clouds (see Hennebelle & Falgarone 2012, for a recent review on the molecular ISM). This outstanding characteristic of the ISM was highlighted by the recent results from the *Herschel* satellite’s far-infrared survey of the inner Galactic plane (e.g., Molinari et al. 2010). On the other hand, a comprehensive analysis of the relative orientation between filamentary interstellar structures and the Galactic magnetic field performed across the whole sky using *Planck* data, has shown that the diffuse interstellar matter is preferentially aligned with the magnetic field, while molecular clouds appear perpendicularly aligned (Planck Collaboration XXXII 2014). Thus, magnetic fields must play an important role in the ISM molecular clouds formation and evolution; nevertheless, understanding its extent and importance in star formation and the competition be-

tween magnetic, and turbulent forces is one of the most heated debate in modern astrophysics (e.g., Mouschovias & Ciolek 1999; Mac Low & Klessen 2004; McKee & Ostriker 2007; Crutcher 2012). Although some theoretical investigations point to supersonic turbulence as the prevailing, possibly the most important, mechanism in the formation of structure and evolution of molecular clouds, most recent results like the one obtained by the *Planck* group and others (e.g., Li et al. 2009, 2013; Vázquez-Semadeni et al. 2011; Soler et al. 2013; Van Loo et al. 2014) testify that the magnetic field is also of crucial importance.

Most of what we know about the plane-of-sky component of the Galactic magnetic field comes from the observation of starlight which is polarized by interstellar dust grains in the foreground. These grains are elongated and according to the pioneering model proposed by Davis & Greenstein (1951) they would be aligned by the magnetic field perpendicular to the field lines. Nevertheless, the paramagnetic relaxation mechanism proposed by Davis & Greenstein exhibits difficulty to reconcile with observations and the actual mechanism responsible for this process has proven to be one of the longest standing problems in astrophysics (see, for instance, Lazarian 2007, for a comprehensive review on the dust alignment theory). Recent advances in this area suggest that radiative torque alignment, originally proposed by Dolginov & Mytrophanov (1976), has become the favored mechanism to explain grain alignment, as showed by models (e.g., Hoang & Lazarian 2014; Hoang et al. 2015) and ob-

* Based on observations collected at Observatório do Pico dos Dias, operated by Laboratório Nacional de Astrofísica (LNA/MCTI, Brazil).

servations (e.g., Alves et al. 2014; Jones et al. 2015). The same aligned dust grains that are responsible for dichroic absorption in the visible and near-infrared wavelengths can emit polarized thermal radiation in the mid- and far-infrared, and radio wavelengths.

The main purpose of this investigation is to study the morphology of the magnetic field in the vicinity of the elongated Lupus I molecular cloud, the most massive cloud ($\sim 1200 M_{\odot}$; Tachihara et al. 1996) in the Lupus complex, a loose conglomerate of dark clouds in the solar vicinity (distant ~ 150 pc according to Crawford 2000; Franco 2002; Alves & Franco 2006; Lombardi et al. 2008). Many young objects from pre-stellar to T Tauri class stars have been associated to these clouds, making them one of the nearest known low-mass star forming regions (for a comprehensive review on the Lupus dark clouds complex see Comerón 2008). Lupus I is particularly interesting because it is the youngest cloud in the complex (Benedettini et al. 2012). This hypothesis is reinforced by the recent census of pre-stellar sources conducted by Rylg et al. (2013) which suggests that Lupus I is currently undergoing a large star formation event.

Earlier references on polarimetric investigations concerning Lupus I can be found in the literature (Myers & Goodman 1991; Rizzo et al. 1998; Matthews et al. 2014). The former two studies are based on optical linear polarization data, while the latter concerns submm polarization data. All of them conclude that in large scale the plane-of-sky component of the magnetic field is perpendicularly aligned to the main axis of Lupus I, like what is observed for many others filamentary molecular clouds (e.g., Heyer et al. 1987; Pereyra & Magalhães 2004; Alves et al. 2008). In this paper we introduce the results from CCD image polarimetry conducted in the R -band for fields with lines-of-sight covering almost the whole area of Lupus I. These data allowed us to go beyond previous works and obtain a detailed description of the configuration of the magnetic field permeating the Lupus I molecular cloud.

2. OBSERVATIONS

The polarimetric data were collected with the 1.6 m and the IAG 60 cm telescopes at Observatório do Pico dos Dias (LNA/MCTI, Brazil) in missions conducted in several nights from 2004 to 2008. The data were obtained with the use of a specially adapted CCD camera to allow polarimetric measurements — for a suitable description of the polarimeter see Magalhães et al. (1996). R -band polarimetry was obtained for 62 fields (with field of view of about $12' \times 12'$ each) covering the main body of the Lupus I molecular cloud and two neighboring diffuse infrared patches. The lines-of-sight of these fields were chosen taking as reference the *IRAS* 100 μm emission map of the region. Among the 62 sky positions, 27 were observed at the IAG 60 cm telescope, and the remaining 35 fields were observed at the 1.6 m telescope. Some of the observed fields overlapped each other, either totally or partially, so that the covered effective area is smaller than the total area covered by the individual frames. In both telescopes the integration time was set to 120 s for each frame, being that at the IAG 60 cm telescope five frames were collected and co-added for each position of the half-wave plate (totalizing 600 s per waveplate position), while at the 1.6 m telescope only one frame was

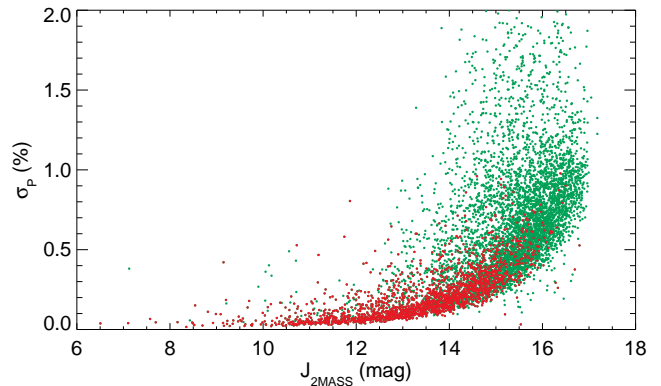


Figure 1. Distribution of the polarimetric errors as a function of the 2MASS J -band magnitude. The red dots represent stars with $P/\sigma_P \geq 5$, while the green dots represent the remaining stars. The distribution shows characteristics of estimated errors dominated by photon shot noise.

obtained for each waveplate position. Most of these observations shared telescope time with a project dedicated to the Pipe Nebula, whose results were previously published elsewhere (Franco et al. 2010). The interested reader is referred to that paper for details on the data reduction, as well as on the observed unpolarized and polarized standard stars used to check for any possible instrumental polarization and for determining the reference direction for the position angles, respectively. The normalized linear polarization is calculated from a least-square solution, which yields the degree of polarization (P), the polarization position angle (θ , measured from north to east), the Stokes parameters Q and U , as well as the theoretical (i.e., the photon noise) and measured errors, σ_{theo} and σ_{fit} , respectively. The latter are obtained from the residuals of the observations at each waveplate position angle (ψ_i) with respect to the expected $\cos 4\psi_i$ curve (see Magalhães et al. 1984, for a brief description on the method used to obtain the least-square solution for the Stokes parameters and the associated errors).

The astrometric calibration was done in two steps. A first solution for each observed frame was obtained from the few stars identified from the Second Digitized Sky Survey (DSS2 red). Such preliminary solution was used to identify stars from the 2MASS catalogue with lines-of-sight toward the frames, and these stars were used to provide a final astrometric solution. This procedure provided accurate coordinates and automatically cross correlated our objects with the 2MASS data catalogue.

Our final polarimetric sample contains about 7000 stars, 1938 of which have $P/\sigma_P \geq 5$, where $\sigma_P = \max\{\sigma_{\text{fit}}, \sigma_{\text{theo}}\}$. In Table 1 we introduce the first 10 lines of our data catalogue for guidance regarding its form and content². Figure 1 gives the distribution of the estimated polarimetric errors, σ_P , as a function of the $J_{2\text{MASS}}$ magnitude. A comparison between data obtained for stars in common to more than one observed frame has shown that the agreement for the measured polarization degree as well as for the position angle were very good. Fig. 2 presents the obtained distribution of the absolute difference between two measurements for

² Table 1 is only available at the CDS via anonymous ftp to cdsarc.u-strasbg.fr (130.79.128.5) or via <http://cdsarc.u-strasbg.fr/viz-bin/qcat?J/ApJ/XXX/XXX>

Table 1
Sample of the polarimetric data obtained for Lupus I

ID	α_{2000} (h m s)	δ_{2000} (° ' ")	l (°)	b (°)	P (%)	σ_{fit} (%)	σ_{theo} (%)	θ (°)	J (mag)	σ_J (mag)	H (mag)	σ_H (mag)	K_S (mag)	σ_{K_S} (mag)
1	15 36 13.79	-33 02 32.4	338.4735	18.2235	0.847	0.132	0.075	89.6	12.145	0.024	11.518	0.021	11.392	0.024
2	15 36 15.85	-33 04 10.7	338.4617	18.1976	1.114	0.411	0.342	123.9	14.775	0.039	14.172	0.044	14.169	0.054
3	15 36 15.86	-33 10 47.0	338.3902	18.1110	1.585	0.186	0.215	102.2	13.814	0.024	13.291	0.021	13.134	0.030
4	15 36 15.98	-33 08 31.0	338.4151	18.1404	1.263	0.010	0.071	85.7	11.939	0.024	11.294	0.023	11.085	0.021
5	15 36 16.07	-33 02 32.2	338.4801	18.2187	0.526	0.353	0.417	21.2	15.131	0.049	14.657	0.046	14.607	0.084
6	15 36 16.22	-33 07 46.7	338.4238	18.1496	1.396	0.441	0.365	99.8	14.915	0.033	14.321	0.044	14.150	0.061
7	15 36 16.28	-33 06 25.2	338.4387	18.1673	1.201	0.215	0.456	128.0	15.387	0.049	14.937	0.079	14.823	0.104
8	15 36 16.29	-33 06 45.5	338.4350	18.1628	1.546	0.436	0.445	91.5	15.105	0.040	14.560	0.063	14.443	0.075
9	15 36 16.78	-33 04 42.1	338.4587	18.1887	0.494	0.293	0.211	99.9	13.935	0.029	13.321	0.030	13.186	0.033
10	15 36 16.88	-33 06 47.6	338.4364	18.1611	0.697	0.147	0.146	109.4	13.753	0.030	13.339	0.030	13.205	0.034

Note. — Table 1 is only available in its entirety at the CDS via anonymous ftp to cdsarc.u-strasbg.fr (130.79.128.5) or via <http://cdsarc.u-strasbg.fr/viz-bin/qcat?J/ApJ/XXX/XXX>. A portion is shown here for guidance regarding its content. Columns, respectively, represent the star's identifier number in our catalogue (ID), the equatorial coordinates (α , δ) retrieved from the 2MASS catalogue, the Galactic coordinates (l , b), the polarization degree (P), together with the two estimated errors for this quantity (the measured (σ_{fit}) and the theoretical (σ_{theo}) errors), the polarization angle (θ), and the 2MASS magnitudes (J , H , K_S) with their associated uncertainties (σ_J , σ_H , σ_{K_S}), respectively.

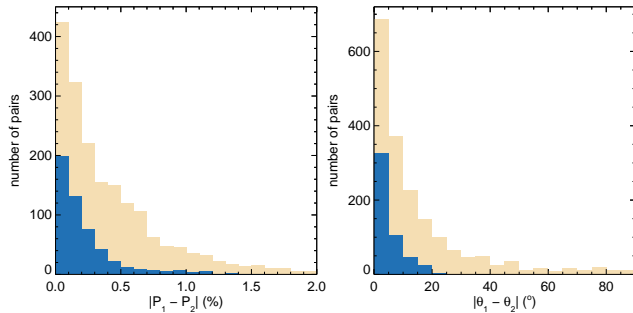


Figure 2. Distribution of the absolute differences in degree of polarization (left) and polarization angles (right) of pairs of measurements for the same star. The wheat histograms give the distribution for all pairs, while the blue histograms are for pairs presenting $P/\sigma_P \geq 5$ only.

the degree of polarization (left panel), $|P_1 - P_2|$, and polarization angles (right panel), $|\theta_1 - \theta_2|$. The histograms coloured in wheat represent the distribution for all observed pairs while the histograms coloured in blue are for pairs of measurements having $P/\sigma_P \geq 5$. Taking into account the latter group we see that the majority of the obtained pairs presents a difference in polarization angle that is ≤ 5 deg, which is consistent with the expected uncertainty for measurements of this quantity ($\sigma_\theta = 28^\circ 65 \sigma_P / P$, Serkowski 1974). It is also seen, for the latter group, that for the majority of the observed pairs the measured difference in degree of polarization is $\leq 0.2\%$.

It is instructive to analyze the 2MASS color-color diagram obtained for the observed stars, shown in Fig. 3. In this diagram the red dots represent stars with $P/\sigma_P \geq 5$, while stars with lower polarimetric measurement quality are represented by the green dots. A large number of stars belonging to this latter group present color indices which are somehow peculiar; it must be noticed, however, that most of them are faint and also have lower photometric quality in the 2MASS catalogue. On the other hand, most of the stars with $P/\sigma_P \geq 5$ have the highest photometric quality in that catalogue. An information we can visually obtain from the 2MASS color-color diagram is that most of the stars observed by our polarimetric survey having $P/\sigma_P \geq 5$ are, in general, probing the outskirts of the dense molecular cloud, with $A_V \leq 5$ mag.

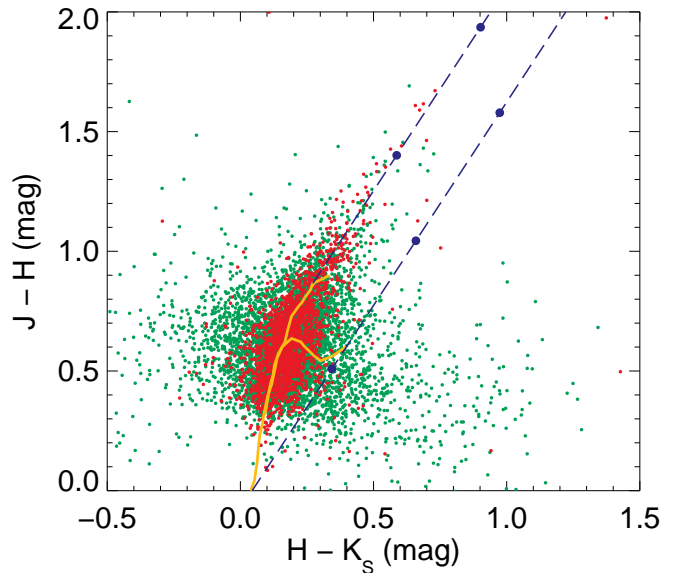


Figure 3. 2MASS $(J-H) \times (H-K_S)$ color-color distribution of the observed stars. The solid curves represent the locus of main-sequence and giant stars and the diagonal dashed lines delimit the normal reddening zone; the large dots show intervals of $A_V = 5$ mag. We used the same color code as in Fig. 1 for representing the data points.

Cambrésy (1999) has estimated peak extinction towards Lupus I of about $A_V \simeq 7.1$ mag, nevertheless more recent estimates of extinction in this cloud indicates $A_V > 20$ mag towards the darkest areas (Benedettini et al. 2012).

3. DATA ANALYSIS

3.1. Large scale morphology of the magnetic field

Hereinafter, only stars having $P/\sigma_P \geq 5$ will be used in our analysis. Figure 4 introduces the distribution of the observed polarization vectors overlaid on the *IRAS* $100 \mu\text{m}$ emission map of Lupus I and its surroundings. In order to complement the information on the surveyed area, we also provide the positions of the different classes of young stellar objects retrieved from Rygl et al. (2013).

The long axis of the main filament of Lupus I is roughly aligned at an angle of 127° east of north, resulting to a normal at about 37° , and at first glance Fig. 4 shows that the large scale plane-of-sky projection of the magnetic

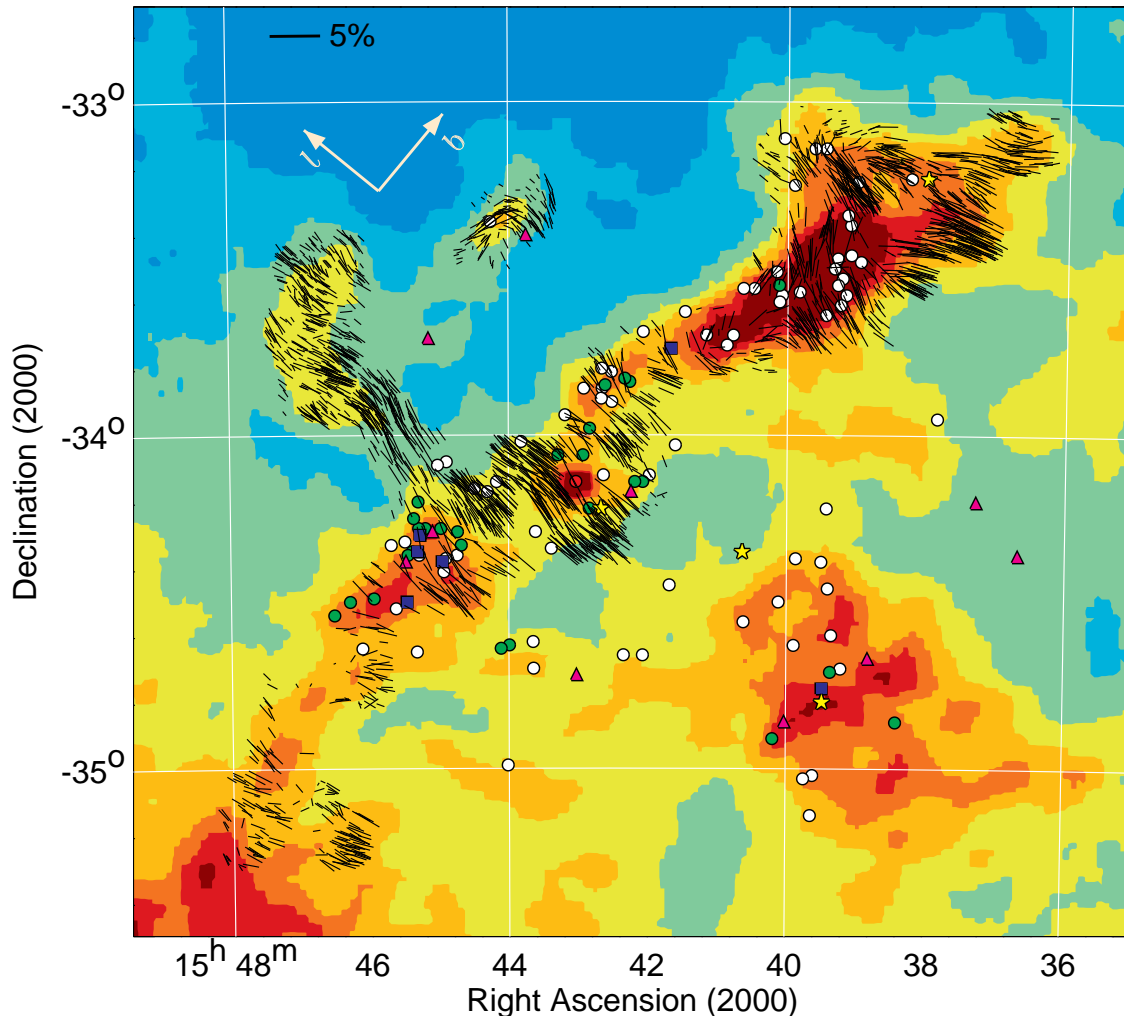


Figure 4. The obtained polarization degree vectors overlaid on the *IRAS* $100\ \mu\text{m}$ emission map of Lupus I and its surrounding region. The length of each vector correlates linearly with the measured degree of polarization according to the scale indicated in the upper left corner, and its orientation gives the direction of the plane-of-sky component of the local magnetic field. The position of different classes of young stellar objects, from Rygl et al. (2013), are indicated according with the following code: unbound cores (white circles), prestellar cores (green circles), class 0 (red circle), class I (triangles), class II (squares), and class III (stars). Directions of increasing Galactic longitude (l) and latitude (b) are shown in the upper left corner.

field appears to be perpendicularly oriented to this main axis, reinforcing the already mentioned previous results (Myers & Goodman 1991; Rizzo et al. 1998; Matthews et al. 2014). Nevertheless, a more detailed inspection suggests the existence of patterns, mainly at the north-western part of the cloud, which is also the region presenting the strongest *IRAS* $100\ \mu\text{m}$ emission. Close to the central part of the cloud, that is, around $15^{\text{h}}43^{\text{m}}$, $-34^{\circ}10'$, the polarization vectors became more uniformly aligned, while in the south-eastern surveyed part of the complex the degree of polarization seems to decrease, compared to the previous regions.

The obtained distribution of the polarization angles has characteristics of a normal distribution centered at 49° , that is, about 12° to the east of the normal to the main axis of Lupus I. The distribution is relatively broad with a standard deviation $\sigma_{\theta} \simeq 19^{\circ}.6$, corresponding to a FWHM $\approx 46^{\circ}$. The obtained values for this distribution agrees perfectly well with the one previously reported by Myers & Goodman (1991), which were obtained from a much smaller sample (98 stars) and Rizzo et al. (1998),

who obtained a mean polarization angle of 52° with a standard deviation $\sigma_{\theta} = 23^{\circ}$, for stars close to the rim of Lupus I.

3.2. Polarization properties

When viewed in Galactic coordinates, the main body of the Lupus I molecular cloud is almost aligned in the north-south direction. We take advantage of this fact to perform a detailed analysis of the distribution of polarization degree and position angles over the main filament and the surrounding infrared patch clouds. Lupus I was observed as part of the *Herschel* Gould Belt survey (André & Saraceno 2005), and although the mapped area is slightly smaller than the one covered by our polarimetric sample, it has a higher angular resolution than the *IRAS* maps and will be useful for the following analysis. In Fig. 5 we display the *Herschel*/SPIRE $350\ \mu\text{m}$ dust emission map obtained for Lupus I³ reprojected in

³ Retrieved from the *Herschel* Gould Belt Survey Archives at <http://gouldbelt-herschel.cea.fr/>

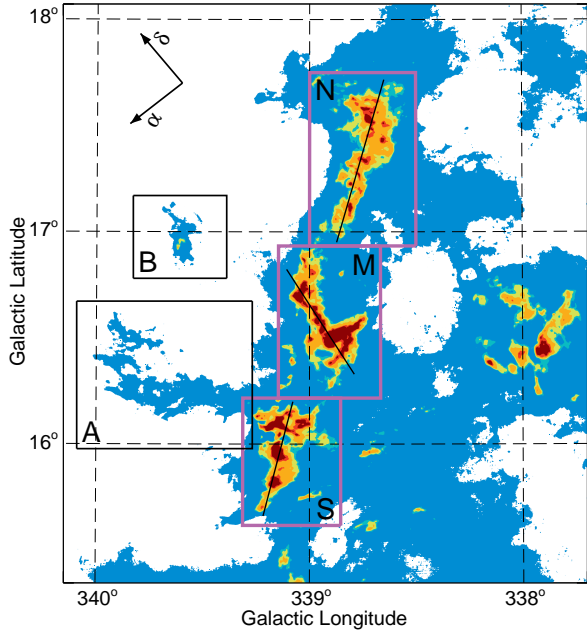


Figure 5. The *Herschel*/SPIRE 350 μm dust emission map for Lupus I. The main filament is dominated by three regions of enhanced emission delimited by the rectangles (colored purple), designated as the “North”, “Middle”, and “South” clumps according to their Galactic latitude. The black lines roughly indicate the direction of the filaments. The two secondary infrared emission patches are delimited by the boxes identified by “A” and “B”. Directions of increasing right ascension (α) and declination (δ) are shown in the upper left corner.

Galactic coordinates. Five regions of interest are delimited by the boxes in this Figure. Three rectangles in the main Lupus I filament delimit regions of enhanced infrared emission that will be referred to as the “North”, “Middle”, and “South” clumps, respectively from north to south. Each of these clumps are elongated, being that the two externals present almost the same direction as the whole filament ($\theta_{\text{gal}} \approx 164^\circ$, east of north), while the middle one, at $\theta_{\text{gal}} \approx 33^\circ$, is tilted by almost 50° in the direction from the north to east.

Interesting results can be obtained when we plot the observed polarization data as a function of the Galactic latitude, as represented in Fig. 6, for the distribution of the observed degree of polarization (upper panel) and the polarization angle (lower panel). Stars having line-of-sight toward the secondary infrared emission patches (boxes “A” and “B” in Fig. 5) were not included in these diagrams.

The vertical dashed-lines delimit the region dominated by each infrared clump. It is clearly seen that although supposedly belonging to the same interstellar structure, the polarimetric characteristics of each clump are distinct. The polarization degree shows a “wavy” distribution, ranging from $\sim 0.3\%$ to little more than 6.0% . In the region located southern of the South clump the degree of polarization does not overpass $\sim 3.0\%$, while it rises in the three infrared clumps suggesting a rather good correlation between degree of polarization and dust emission.

More interesting is the distribution of polarization angles as a function of the Galactic latitude. Polarization measured for stars located northern of the North clump present most of their position angles within the range

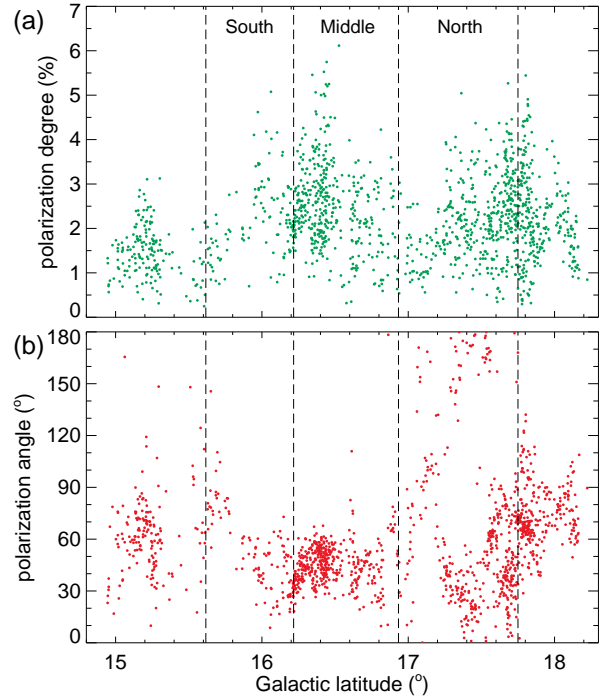


Figure 6. Distribution of the degree of polarization (upper panel) and polarization angles (lower panel) as a function of the Galactic latitude for stars towards the “main filament”. The vertical dashed lines delimit the latitudes separating the regions defined in Fig. 5 for the main filament.

from $\sim 50^\circ$ to 110° . Then, inside the latitudes limiting the vicinity of the North clump we obtained basically any polarization angles, with a tendency of concentration around $30^\circ \pm 20^\circ$. In the range of latitudes delimiting the Middle clump, we see a narrow distribution centered around $\sim 40^\circ$, while in the South clump the position angles show a tendency to increase with decreasing Galactic latitude.

Some of these properties are better seen in the histograms introduced in Fig. 7. The distributions were obtained using stars having lines-of-sight through the regions delimited by the rectangles shown in Fig. 5 only. The vertical dashed-lines indicate the visual estimated position angle of the normals to the infrared clumps, which for both, the North and South clumps, are basically the same as to the whole Lupus I filament, while for the Middle clump, it is tilted by almost 50° with relation to the former one. Right-hand panel, gives the distribution obtained for stars in the North clump region, and as anticipated by the observed distribution of polarization angles as function of the Galactic latitude, the full range of angles are somehow encompassed, nevertheless with a clear component almost centered perpendicularly to the infrared clump long axis. Middle panel, displays the obtained distribution for stars with lines-of-sight through the Middle clump region, and the distribution resembles a normal distribution as evidenced by the fitted Gaussian (center at $\sim 46^\circ$ and a quite narrow width $\sigma = 11^\circ$). The obtained angle for the center of this distribution is basically identical to the one obtained for the full sample, that is, almost perpendicular to the long axis of Lupus I, however shifted about 40° from the supposed normal to the local infrared clump. Finally, left-hand panel, dis-

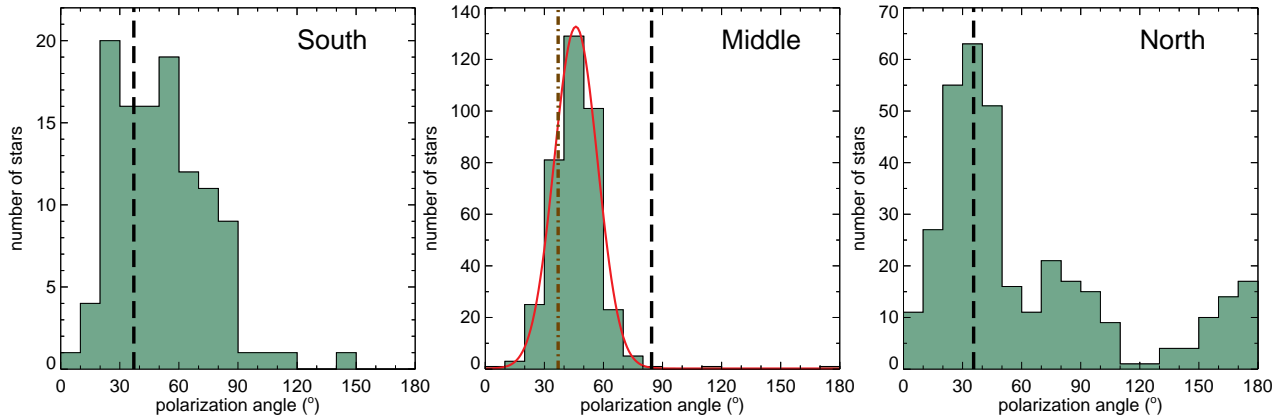


Figure 7. Distribution of the polarization angles. *Left-hand panel* displays the obtained distribution for stars inside the southern box as defined in Fig. 5. The vertical dashed-line indicates the estimated orthogonal orientation to the main axis of the clump. Middle panel, same as left-hand panel, but for the middle box. The fitted Gaussian centered at $\sim 46^\circ$ and a standard deviation of 11° shows that the observed distribution resembles a normal one, and presents a small dispersion. The vertical dot-dashed line indicates the orthogonal orientation to the main Lupus I filament. The *right-hand panel* displays the observed distribution for stars inside the northern box. The obtained distribution covers almost all interval of angles, nevertheless, the main peak in the distribution coincides with the direction perpendicular to the longest axis of the clump.

plays the obtained distribution for stars with line-of-sight through the South clump region. Although the observed polarization angles do not cover the full range like what was obtained for the North clump, this region presents a broad distribution probably due to a merger of different magnetic field components.

3.3. The optical polarization on the infrared diffuse patches

As mentioned before, our polarimetric survey also covered two adjoining low infrared emission clouds at the Lupus I region. The one delimited in Fig. 5 by the rectangle designed by “A” corresponds to the northern part of the secondary filament also labeled “A” by Matthews et al. (2014, see their Fig. 3). As noted by these authors, this secondary filament is perpendicularly aligned to the main Lupus I filament. Fig. 8 gives a detailed map of the observed polarization overlaid on the *Herschel*/SPIRE $350\ \mu\text{m}$ dust emission for this filament and for the other small diffuse infrared clump delimited by the rectangle designed “B” in Fig. 5. The similarity between the features shown by the distribution of dust emission and the orientation of the polarization vectors is remarkable, the former seems to follow perfectly the field configuration.

Matthews et al. (2014) have already noted that the extension of the secondary filament A south of the main Lupus I dust cloud (not covered by our data), was aligned to their submm polarization vectors. Our results reinforce their suggestion that Lupus I consists of a dominant filament running orthogonally to the mean magnetic field, surrounded by secondary filaments that run parallel to their local field directions. This is in agreement with the recent results obtained by Planck Collaboration XXXII (2014) that diffuse interstellar structures are preferentially aligned with the magnetic field, while dense molecular clouds appear orthogonally oriented to the magnetic fields.

A question that comes to mind is if secondary filament A is nourishing the main dust filament. Unfortunately, our data does not allow to go further to this point, however, unless the material composing these filaments are distributed on the plane-of-sky, a detailed kinematical

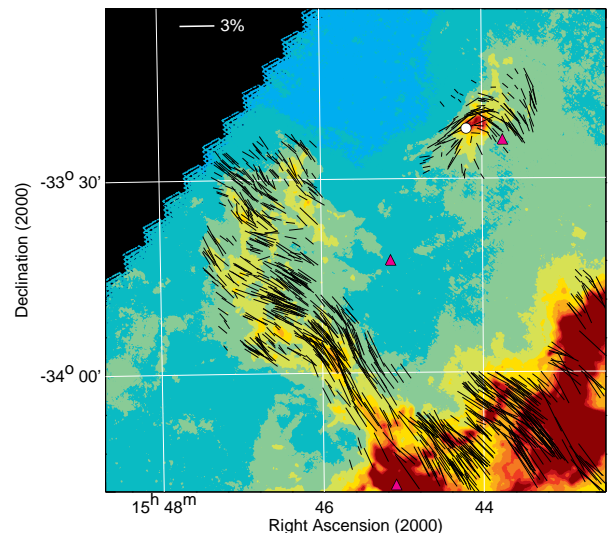


Figure 8. Detail of the distribution of the linear polarization vectors overlaid on the *Herschel*/SPIRE $350\ \mu\text{m}$ emission map. The symbols have the same meaning as in Fig. 4. The black area at the upper left corresponds to a region not covered by the *Herschel* survey.

investigation of them would be interesting.

While no prestellar object has been so far found in the surveyed area covering the diffuse filament A, an unbound core and a Class I object were found associated with patch B, the former sits in the densest part of the infrared emission observed for this patch. The interesting feature observed, for the magnetic field in the region, is its elbow like structure. The reason for this abrupt bending in the local magnetic field may be associated to the physical processes leading to the formation of the two young stellar objects found in this area. Further higher resolution observations are needed in order to verify that.

3.4. Angular Dispersion Function, Magnetic Field Strength, and cloud stability

3.4.1. The angular dispersion function

Our polarization map provides the quality and angular resolution to apply the method of Hildebrand et al.

(2009) for estimating the plane-of-sky component of the magnetic field acting on the Lupus I molecular cloud. In their method they use the difference in angle, $\Delta\Phi(\ell) \equiv \Phi(\mathbf{x}) - \Phi(\mathbf{x} + \ell)$, between the $N(\ell)$ pairs of vectors separated by displacements ℓ , to compute the angular dispersion function, ADF, defined as:

$$\langle \Delta\Phi^2(\ell) \rangle^{1/2} \equiv \sqrt{\frac{1}{N(\ell)} \sum_{i=1}^{N(\ell)} [\Phi(\mathbf{x}) - \Phi(\mathbf{x} + \ell)]^2}. \quad (1)$$

They consider that the magnetic field is composed of a large-scale structured field, $\mathbf{B}_0(\mathbf{x})$, and a turbulent component, $\mathbf{B}_t(\mathbf{x})$, and because the former is a smoothly varying quantity, its contribution to the dispersion function should increase linearly with ℓ for small distances. That is, they show that the square of the ADF can be approximated by

$$\langle \Delta\Phi^2(\ell) \rangle_{\text{tot}} \simeq b^2 + m^2\ell^2 + \sigma_M^2(\ell) \quad (2)$$

where $\sigma_M(\ell)$ represents the contribution due to measurements uncertainties on the polarization angles and b the turbulent contribution to the angular dispersion, expected to maintain constant, as long as ℓ is larger than the correlation length characterizing $\mathbf{B}_t(\mathbf{x})$.

Figure 9 displays the obtained ADF for the three clumps of the main Lupus I filament. In computing that we used only polarization data for stars inside the boxes shown in Fig. 5. At first glance we note that the turbulent contribution, b , in all three clumps is rather small implying that the ratio of the turbulent to large-scale magnetic field strength, given by (see, Hildebrand et al. 2009)

$$\frac{\langle B_t^2 \rangle^{1/2}}{B_0} = \frac{b}{\sqrt{2 - b^2}} \quad (3)$$

is significantly less than 1 (see column 3 of Table 2), indicating that turbulence is less important than the magnetic fields in these parts of the cloud.

The strength of the plane-of-sky component of the magnetic field may be estimated by a modified version of the classical method proposed by Chandrasekhar & Fermi (1953, hereafter CF). These authors assumed equipartition between kinetic and perturbed magnetic energies to assert that the dispersion in polarization angles, $\delta\theta$, together with the dispersion in velocity along the line-of-sight, δV , can reveal information about the magnitude of the magnetic field. Following the original derivation of CF, an equation for the mean value of the plane-of-sky component of the magnetic field can be written as

$$B_{\text{pos}} = Q\sqrt{4\pi\rho} \frac{\delta V}{\delta\theta} \quad (4)$$

where ρ is the mass density, and Q is a scale factor that equals to unity in the CF model, however effects not included in the original formula, such as inhomogeneity and averaging several turbulent cells, among others (see for instance, Zweibel 1996), tend to overestimate the value of the field strength. Studies based on simulations suggest that $Q \approx 0.5$ can yield reliable values of B_{pos} ,

provided the dispersion in angle is less than $\sim 25^\circ$ (e.g., Ostriker et al. 2001; Heitsch et al. 2001; Padoan et al. 2001). Adopting $Q = 0.5$ and using $\rho = mn_{H_2}$ and $\Delta V = \sqrt{8 \ln 2} \delta V$, where n_{H_2} is the molecular hydrogen density in molecules cm^{-3} and ΔV the FWHM line width in km s^{-1} , we obtain (Crutcher et al. 2004)

$$B_{\text{pos}} \approx 9.3\sqrt{n_{H_2}} \frac{\Delta V}{\delta\theta} \quad (5)$$

and using the identity $b^2 \approx 2\delta\theta^2$, that follows from Eq. (3) when $b^2 \ll 2$ (Hildebrand et al. 2009),

$$B_{\text{pos}} = 9.3 \left(\frac{2n_{H_2}}{\text{cm}^{-3}} \right)^{1/2} \left(\frac{\Delta V}{\text{km s}^{-1}} \right) \left(\frac{b}{1^\circ} \right)^{-1} \mu\text{G} \quad (6)$$

3.4.2. Gas density and velocity line width

In order to obtain the plane-of-sky component of the large-scale magnetic field we need to know the values of the gas density and velocity line width toward the investigated line-of-sight. To estimate the gas density we assume some hypothesis that will be responsible for the main uncertainty in the obtained value of the strength of the plane-of-sky component of the magnetic field. Visual extinctions, A_V , may be converted to molecular hydrogen column density by using the canonical relation $N(H_2) = 9.4 \times 10^{20} A_V \text{ cm}^{-2} \text{ mag}^{-1}$ suggested by Bohlin et al. (1978), and to molecular density by assuming a line-of-sight cloud's thickness. However, there is not a precise way to infer the thickness. Recent investigations conducted in different star forming clouds suggest that filaments are typically very long, with lengths of ~ 1 pc or more, and a possible similar characteristic width of ~ 0.1 pc (Arzoumanian et al. 2011; André et al. 2014), that is, filamentary clouds may be modelled by an idealized cylindrical filament with radial density and column density profiles.

The mean visual extinction towards the observed stars in each of the three clumps' areas was estimated using the extinction map based on the 2MASS PSC created by Dobashi (2011)⁴ and is given in column 4 of Table 2. It must be noted that many lines-of-sight returned negative values for the visual extinction, and that these data values were not considered in our averaging process. Also, many observed stars present degree of polarization much higher than the one expected by the optimum alignment relation $P_V \approx 3.0 A_V \% \text{ mag}^{-1}$, suggesting that the visual extinction obtained from Dobashi's map, for these lines-of-sight, may be slightly underestimated. Another sign that the visual extinction retrieved from Dobashi's map for our stellar sample may be underestimated for some lines-of-sight is that Franco (2002), in an investigation of the surroundings of Lupus I, found that stars towards directions having *IRAS* 100 μm emission above 28 MJy sr^{-1} , which is the case for the majority of the stars observed in this work, present a minimum color excess of $E(b - y) \approx 0.1 \text{ mag}$, corresponding to $A_V \approx 0.4 \text{ mag}$.

To estimate the molecular density we adopted a distance of 150 pc to the clumps and the width of the boxes

⁴ <http://darkclouds.u-gakugei.ac.jp>

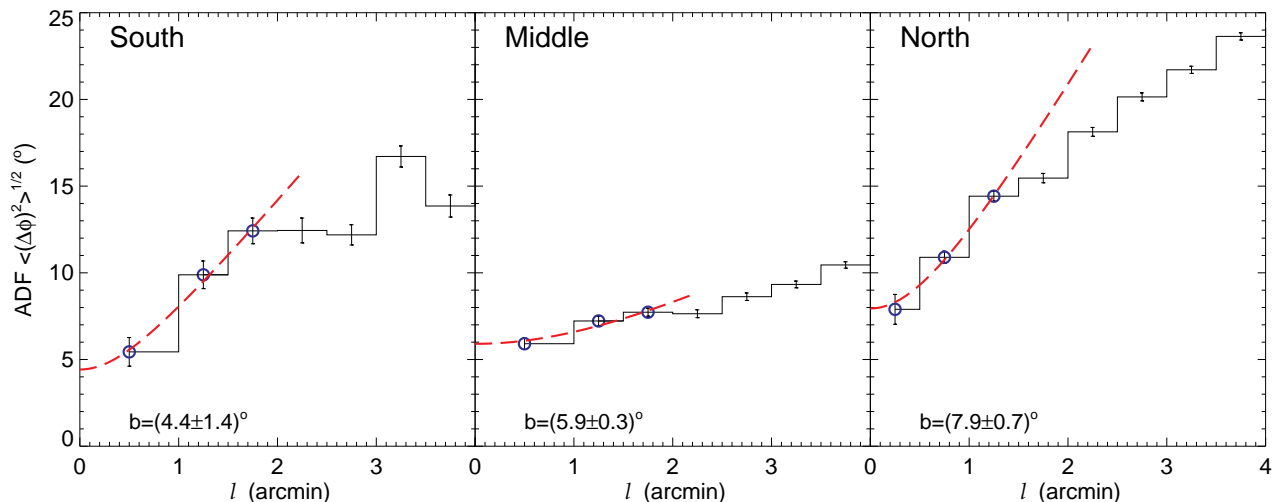


Figure 9. Plot of the angular dispersion function, $\langle \Delta\Phi^2(\ell) \rangle^{1/2}$, for the three clumps of the main Lupus I molecular cloud filament. We considered only polarization vectors inside the rectangles shown in Fig. 5 in calculating these functions. In order to reduce the errors, indicated by the vertical bars, the first bin in the diagrams for the South and Middle clumps were adopted as having twice the size ($1'$) of the others bins. The best-fit to the three first data points are shown by the dashed curves. The turbulent contribution to the total angular dispersion is determined by the zero intercept of the best-fit at $\ell = 0$, and the obtained value is given at the lower left-hand corner of each panel. The measurement uncertainties, that is, the term $\sigma_M(\ell)$ in the right-hand side of Eq. 2, were removed prior to operating the fits to the corresponding data sets.

shown in Fig. 5 as the thickness of the absorbing material. The obtained densities are given in column 5 of Table 2. Although the uncertainties in the estimated column density and adopted cloud thickness, the values we obtained for the molecular density seem reasonable when compared with the ones obtained in the Taurus molecular clouds. If we accept that the same physical conditions prevailing in those clouds are also valid in Lupus I, then we would expect a minimum $n(H_2) \approx 375 \text{ cm}^{-3}$ for lines-of-sight where ^{12}CO is detected (see, Pineda et al. 2010), meaning that in the worst case, the obtained values give the lower limit for the molecular hydrogen density in the surveyed areas.

Unlike the molecular density, the velocity line width is a quantity that does not depend on a priori assumptions, however, the choice of which data to use contribute to uncertainties in the final determination of the strength of the plane-of-sky component of the magnetic field. The Lupus molecular clouds were mapped a number of times in different molecular lines, however, in general, none of the data provided in the literature covers exactly our studied regions. For example, Tachihara et al. (1996) obtained $\Delta V = 1.9 \text{ km s}^{-1}$ for $^{13}\text{CO } J = 1 \rightarrow 0$ at the peak of integrated intensity for Lupus I, and Murphy et al. (1986) give $\Delta V = 3.55 \text{ km s}^{-1}$ at ($l = 338^\circ 5$, $b = 17^\circ 5$) and $\Delta V = 2.66 \text{ km s}^{-1}$ at ($l = 339^\circ 0$, $b = 16^\circ 0$), two direction towards our mapped area, for $^{12}\text{CO } J = 1 \rightarrow 0$. In this work we opted by using the $^{13}\text{CO } J = 2 \rightarrow 1$ line widths obtained by Tothill et al. (2009). They observed three lines-of-sight towards the northern clump, eight towards the middle clump, and three towards the southern clump, respectively. It must be noted that these measurements were gathered for high column density lines-of-sight in these clumps, while we are surveying the outskirts of the clumps. For each region we adopted the mean value of the velocity line width as given in column 6 of Table 2. Tothill et al. (2009) also provide $^{12}\text{CO } J = 4 \rightarrow 3$ line width for the same lines-of-sight. The

mean values of these lines differ from the ones adopted by 10-15%, being larger for the northern clump and smaller for the others two.

The obtained plane-of-sky magnitudes of the large-scale magnetic field are given in column 7 of Table 2. We note, however, that these values should be taken as an estimation only of the actual magnetic field strength, due to uncertainties in the adopted quantities. Although the error is dominated by uncertainties in the determination of the molecular hydrogen density n_{H_2} , we must take into account also the uncertainties in measured line width, the estimated b parameter, and the scale factor Q , assumed as equal to 0.5.

3.4.3. Cloud stability

It is also interesting to investigate the stability of the studied clumps. According to Nakano & Nakamura (1978) the critical value for the mass that can be supported by a magnetic flux Φ is $M_{B,\text{crit}} = \Phi/2\pi G^{1/2}$. The ratio of the mass to the magnetic flux is then a crucial parameter that can supply information on the support and stability of the interstellar clouds. A dimensionless parameter $\lambda \equiv (M/\Phi)_{\text{actual}}/(M/\Phi)_{\text{crit}}$, can be estimated using the molecular hydrogen density and the magnetic field strength by (Crutcher et al. 2004)

$$\lambda = \frac{(M/\Phi)_{\text{observed}}}{(M/\Phi)_{\text{crit}}} = \frac{mNA/BA}{1/2\pi\sqrt{G}} = 7.6 \times 10^{-21} \frac{N_{\parallel}(H_2)}{B_{\text{tot}}} \quad (7)$$

where N_{\parallel} is the column density along the magnetic flux tube in units of cm^{-2} and B_{tot} is the total magnetic field strength given in μG . As demonstrated by Heiles & Crutcher (2005), $\langle N_{\text{obs}}/B_{\text{pos}} \rangle = 3\langle N_{\parallel}/B_{\text{tot}} \rangle$, i.e., using statistical arguments they show that in average the observed ratio between column density and the plane-of-sky magnetic field overestimates the ratio used in Eq. (7) by a factor of three. Thus, we can use our previous estimates of molecular column density and plane-of-sky

Table 2
Obtained physical parameters for the three clumps in the main Lupus I filament (see text for details)

Clump	b ($^{\circ}$)	$\langle B_t^2 \rangle^{1/2}/B_0$	$\langle A_V \rangle^a$ mag	n_{H_2} (cm^{-3})	ΔV^b (km s^{-1})	B_{pos} (μG)	λ
North	7.9 ± 0.7	0.10 ± 0.01	1.80	418	2.2	75	0.057
Middle	5.9 ± 0.3	0.08 ± 0.01	1.93	466	2.3	111	0.041
South	4.4 ± 1.4	0.05 ± 0.02	2.13	540	2.7	188	0.027

^a Based on the extinction map created by Dobashi (2011)

^b $^{13}\text{CO } J = 2 \rightarrow 1$ line width from Tothill et al. (2009)

magnetic field to estimate the λ parameter, provided we divide it by 3.

The obtained results for all three clumps in the main filament of Lupus I indicate that their inferred mass-to-magnetic flux ratios are subcritical (see last column of Table 2). That means, in large scale, this molecular cloud is magnetically supported as would be expected for a filament perpendicularly aligned with the field lines. Nevertheless, the mass of the main filament of Lupus I may be increasing due to a possible longitudinal mass movement of the material in the secondary infrared interstellar patches that seems to be channeling into the main filament along the field lines.

In spite of the fact that the parameter b , and consequently the ratio of the turbulent to the large-scale magnetic field strength, and the mass-to-magnetic flux ratio obtained for all three clumps being rather similar, the large-scale magnetic field morphology in these clumps are not. As already noticed, these differences are clearly observed in the histograms given in Fig. 7, and are also clear in the ADF plots shown in Fig. 9. The large-scale structure is described in Equation (2) by the term $m\ell$, which is much steeper for the North clump and less for the Middle clump.

It is also interesting to note that a large fraction of the cores and young stellar object found in Lupus I are located in these clumps, and that their distribution is not uniform (see Fig. 4). Basically all objects found in the North clump seem to be unbound objects, that is, objects having ratio of the core mass to its critical Bonnor-Ebert mass less than 1, suggesting that they may or may not form stars. On the other hand, in the Middle clump, apart from some supposedly unbound cores, there are also several prestellar (bounded) cores and a couple of more evolved objects (Class 0 and I). The South clump seems to be the most evolved one, containing several Class I and II objects. All together, it suggests a sequence where the southern end of the cloud is more evolved than the middle which in turn is more evolved than the northern end. Although we may suspect that there exists a correlation between this fact and the observed characteristics of the large-scale magnetic field exerting on the clumps, it is not possible to assert that based only in our results.

4. CONCLUSIONS

We have analyzed the R -band imaging linear polarimetry data obtained for background stars in the region of the Lupus I molecular cloud. Despite the global results are similar to ones obtained in previous investigations, the higher angular resolution of our data allowed us to obtain new information not investigated before. Our

main results are as follow.

1. The large scale map of the plane-of-sky magnetic field shows that the main filament of Lupus I is normally oriented to the field, reinforcing previous investigations that found the same (e.g. Myers & Goodman 1991; Rizzo et al. 1998; Matthews et al. 2014). On the other hand, this map also shows that two small diffuse infrared clouds in the neighborhood of the main filament are parallel to the field lines.
2. When the polarization data are analyzed as a function of the stellar position on the plane-of-sky, some interesting features are observed, mainly concerning the distribution of polarization angles as a function of the Galactic latitude. The observed characteristic feature seems to be somehow related to the clumps of interstellar material.
3. The ratio of the turbulent to the large-scale magnetic field strength obtained for three major clumps in Lupus I is significantly less than 1, implying that in this cloud the turbulence is less important than the large-scale magnetic fields.
4. The estimated strength of the plane-of-sky component of the large-scale magnetic field ranges from ~ 70 to $\sim 200 \mu\text{G}$ for the North to the South clumps, respectively. Nevertheless, the reader should bear in mind that these values are very sensitive to the adopted quantities characterizing the properties of the probed interstellar medium.
5. There is evidence that the clumps are magnetically supported on large scales. This is in agreement with the observational fact that the gas and dust composing the main structure of Lupus I have collapsed along the field lines to form a filament. There is also evidence that this process is still ongoing by the accretion of material along field lines like what is suggested by the result obtained for one of the observed diffuse infrared patches.

The results introduced here and the fact that Lupus I is currently undergoing a large star formation event (Rygl et al. 2013), make this cloud an interesting site for future investigations on the importance of magnetic fields in the star formation process.

We thank the referee for her/his insightful and valuable comments that substantially improved our paper. We thank the staff of the Observatório do Pico dos Dias

(LNA/MCTI, Brazil) for their hospitality and invaluable help during our observing runs. This research has made use of the NASA/IPAC Infrared Science Archive, which is operated by the Jet Propulsion Laboratory, California Institute of Technology, under contract with the National Aeronautics and Space Administration through the use of data products from the Two Micron All Sky Survey, which is a joint project of the University of Massachusetts and the Infrared Processing and Analysis Center/California Institute of Technology, funded by the National Aeronautics and Space Administration and the National Science Foundation and from the *Infrared Astronomical Satellite* which was a joint project of the US, UK and the Netherlands. This research has made use of data from the Herschel Gould Belt survey (HGBS) project. The HGBS is a Herschel Key Programme jointly carried out by SPIRE Specialist Astronomy Group 3 (SAG 3), scientists of several institutes in the PACS Consortium (CEA Saclay, INAF-IFSI Rome and INAF-Arcetri, KU Leuven, MPA Heidelberg), and scientists of the Herschel Science Center (HSC). This research has also made use of the Digitized Sky Survey produced at the Space Telescope Science Institute under U.S. Government grant NAG W-2166, which is based on photographic data obtained using the UK Schmidt Telescope and the Palomar Sky Survey. We have also made extensive use of NASA's Astrophysics Data System (NASA/ADS) and the SIMBAD database, operated at CDS, Strasbourg, France. We are grateful to Drs. A. M. Magalhães and A. Pereyra for supplying us with the polarimetric unit and the software used for data reductions. This research has been partially supported by CNPq and FAPEMIG.

Facilities: LNA: 1.6 m and BC0.6 m

REFERENCES

- Alves, F. O. & Franco, G. A. P. 2006, *MNRAS*, 366, 238
 Alves, F. O., Franco, G. A. P., & Girart, J. M. 2008, *A&A*, 486, L13
 Alves, F. O., Frau, P., Girart, J. M., et al. 2014, *A&A*, 569, L1
 André, P., Di Francesco, J., Ward-Thompson, D., et al. 2014, *Protostars and Planets VI*, 27
 André, P. & Saraceno, P. 2005, in *ESA Special Publication*, Vol. 577, *ESA Special Publication*, ed. A. Wilson, 179–184
 Arzoumanian, D., André, P., Didelon, P., et al. 2011, *A&A*, 529, L6
 Benedettini, M., Pezzuto, S., Burton, M. G., et al. 2012, *MNRAS*, 419, 238
 Bohlin, R. C., Savage, B. D., & Drake, J. F. 1978, *ApJ*, 224, 132
 Cambrésy, L. 1999, *A&A*, 345, 965
 Chandrasekhar, S. & Fermi, E. 1953, *ApJ*, 118, 113
 Comerón, F. 2008, *Handbook of Star Forming Regions*, Volume II: The Southern Sky, Edited by Reipurth, B. (*ASP Monograph*), 295
 Crawford, I. A. 2000, *MNRAS*, 317, 996
 Crutcher, R. M. 2012, *ARA&A*, 50, 29
 Crutcher, R. M., Nutter, D. J., Ward-Thompson, D., & Kirk, J. M. 2004, *ApJ*, 600, 279
 Davis, L. J. & Greenstein, J. L. 1951, *ApJ*, 114, 206
 Dobashi, K. 2011, *PASJ*, 63, 1
 Dolginov, A. Z. & Mytrophanov, I. G. 1976, *Ap&SS*, 43, 257
 Franco, G. A. P. 2002, *MNRAS*, 331, 474
 Franco, G. A. P., Alves, F. O., & Girart, J. M. 2010, *ApJ*, 723, 146
 Heiles, C. & Crutcher, R. 2005, in *Lecture Notes in Physics*, Berlin Springer Verlag, Vol. 664, *Cosmic Magnetic Fields*, ed. R. Wiebeinski & R. Beck, 137
 Heitsch, F., Zweibel, E. G., Mac Low, M.-M., Li, P., & Norman, M. L. 2001, *ApJ*, 561, 800
 Hennebelle, P. & Falgarone, E. 2012, *A&A Rev.*, 20, 55
 Heyer, M. H., Vrba, F. J., Snell, R. L., et al. 1987, *ApJ*, 321, 855
 Hildebrand, R. H., Kirby, L., Dotson, J. L., Houde, M., & Vaillancourt, J. E. 2009, *ApJ*, 696, 567
 Hoang, T. & Lazarian, A. 2014, *MNRAS*, 438, 680
 Hoang, T., Lazarian, A., & Andersson, B.-G. 2015, *MNRAS*, 448, 1178
 Jones, T. J., Bagley, M., Krejny, M., Andersson, B.-G., & Bastien, P. 2015, *AJ*, 149, 31
 Lazarian, A. 2007, *J. Quant. Spec. Radiat. Transf.*, 106, 225
 Li, H.-b., Dowell, C. D., Goodman, A., Hildebrand, R., & Novak, G. 2009, *ApJ*, 704, 891
 Li, H.-b., Fang, M., Henning, T., & Kainulainen, J. 2013, *MNRAS*, 436, 3707
 Lombardi, M., Lada, C. J., & Alves, J. 2008, *A&A*, 480, 785
 Low, F. J., Young, E., Beintema, D. A., et al. 1984, *ApJ*, 278, L19
 Mac Low, M.-M. & Klessen, R. S. 2004, *Reviews of Modern Physics*, 76, 125
 Magalhães, A. M., Benedetti, E., & Roland, E. H. 1984, *PASP*, 96, 383
 Magalhães, A. M., Rodrigues, C. V., Margoniner, V. E., Pereyra, A., & Heathcote, S. 1996, in *ASP Conf. Ser. 97: Polarimetry of the Interstellar Medium*, 118
 Matthews, T. G., Ade, P. A. R., Angilè, F. E., et al. 2014, *ApJ*, 784, 116
 McKee, C. F. & Ostriker, E. C. 2007, *ARA&A*, 45, 565
 Molinari, S., Swinyard, B., Bally, J., et al. 2010, *A&A*, 518, L100
 Mouschovias, T. C. & Ciolek, G. E. 1999, in *NATO ASIC Proc. 540: The Origin of Stars and Planetary Systems*, ed. C. J. Lada & N. D. Kylafis, 305
 Murphy, D. C., Cohen, R., & May, J. 1986, *A&A*, 167, 234
 Myers, P. C. & Goodman, A. A. 1991, *ApJ*, 373, 509
 Nakano, T. & Nakamura, T. 1978, *PASJ*, 30, 671
 Ostriker, E. C., Stone, J. M., & Gammie, C. F. 2001, *ApJ*, 546, 980
 Padoan, P., Goodman, A., Draine, B. T., et al. 2001, *ApJ*, 559, 1005
 Pereyra, A. & Magalhães, A. M. 2004, *ApJ*, 603, 584
 Pineda, J. L., Goldsmith, P. F., Chapman, N., et al. 2010, *ApJ*, 721, 686
 Planck Collaboration XXXII. 2014, *ArXiv e-prints:1409.6728*
 Rizzo, J. R., Morras, R., & Arnal, E. M. 1998, *MNRAS*, 300, 497
 Rygl, K. L. J., Benedettini, M., Schisano, E., et al. 2013, *A&A*, 549, L1
 Serkowski, K. 1974, in *Methods Exper. Phys. Vol. 12A*, ed. N. Carleton (Academic, New York), 361
 Soler, J. D., Hennebelle, P., Martin, P. G., et al. 2013, *ApJ*, 774, 128
 Tachihara, K., Dobashi, K., Mizuno, A., Ogawa, H., & Fukui, Y. 1996, *PASJ*, 48, 489
 Tothill, N. F. H., Löhr, A., Parshley, S. C., et al. 2009, *ApJS*, 185, 98
 Van Loo, S., Keto, E., & Zhang, Q. 2014, *ApJ*, 789, 37
 Vázquez-Semadeni, E., Banerjee, R., Gómez, G. C., et al. 2011, *MNRAS*, 414, 2511
 Zweibel, E. G. 1996, in *Astronomical Society of the Pacific Conference Series*, Vol. 97, *Polarimetry of the Interstellar Medium*, ed. W. G. Roberge & D. C. B. Whittet, 486